X-Ray Polarimetry With a Micro Pattern Gas Detector With Pixel Readout

R. Bellazzini, F. Angelini, L. Baldini, A. Brez, E. Costa, L. Latronico, N. Lumb, M. M. Massai, N. Omodei, P. Soffitta, and G. Spandre

***Abstract*—In astronomy there are basically four kinds of observations to extract the information carried by electromagnetic radiation: photometry, imaging, spectroscopy, and polarimetry. By optimal exploitation of the first three techniques, X-ray astronomy has been able to unveil the violent world of compact high-energy sources. Here, we report on a new instrument that brings high efficiency also to X-ray polarimetry, the last unexplored field of X-ray astronomy. It will then be possible to resolve the internal structures of compact objects, which otherwise would remain inaccessible even to X-ray interferometry. The new instrument derives the polarization information from the track of the photoelectron imaged by a finely subdivided gas pixel detector. Its great improvement of sensitivity (at least two order of magnitude) will allow direct exploration of the most dramatic objects of the X-ray sky.**

***Index Terms*—Gas detectors, polarimetry, X-ray.**

I. Introduction

A significant degree of linear polarization can be expected in a large number of astrophysical X-ray sources due either to the emission processes themselves (for example synchrotron radiation) or to the interaction of primary (unpolarized) photons, with the matter surrounding the emitting region. Thomson scattering on aspherical accreting plasmas is a typical example of this second possibility, explaining why radiation coming from systems with accretion disks should be polarized [1]; in this case, X-ray polarimetry could determine the orientation of the disk with respect to the line of sight. In addition to this, the observation of the characteristic twisting of the polarization angle as a function of photon energy due to gravitational bending in compact sources [2] would constitute a definitive test of the existence of a black hole. In the case of binary X-ray pulsars (magnetized spinning neutron stars accreting from a near companion), a degree of polarization as high as 80% is expected [3] due to the different opacity of a strongly magnetized plasma to photons polarized along the magnetic field and orthogonally to it; the detection of this polarization (and its variations with the pulse phase) would determine the geometrical features of the accreting matter and provide a measurement of the angle between the magnetic axis and the rotation axis of the star.

So far, the detection of the polarization of the Crab Nebula [5], dating from more than 25 years ago, is the only universally accepted result of astronomical X-ray polarimetry. Apart from this, basically for a lack of adequate instrumentation, observations have provided only weak upper limits on a few sources—not enough to allow a real comparison with theory. As outlined by Meszaros [4], efficient polarimetry would add two further observable quantities (the amount and angle of polarization) to the parameter space of X-ray astronomy and would lead to a very significant improvement in our ability to discriminate between various possible theoretical models.

In this paper, we report the development of a new highly efficient polarimeter based on the photoelectric effect, for the 2–10 keV energy range (a particularly interesting band for X-ray astronomers). We derive the polarization information from the tracks of the photoelectrons, reconstructed with a finely segmented gas detector with pixel readout.

II. The Instrument

The photoelectric effect is very sensitive to polarization; the photoemission differential cross section for a K-shell electron, in the nonrelativistic limit is given by [6]

$$\frac{d\sigma}{d\Omega} = r_0^2 Z^5 \alpha^4 \left(\frac{m_e c^2}{h\nu}\right)^{\frac{7}{2}} \frac{4\sqrt{2}\sin^2\theta\cos^2\phi}{(1-\beta\cos\theta)^4} \qquad (1)$$

where θ is the polar angle with respect to the wave vector $\mathbf{k}$ of the incoming photon, ϕ is the azimuthal angle with respect to its polarization direction (Fig. 1), Z is the atomic number of the absorption material, and β is the speed of the electron (in units of c). We should notice that in the plane orthogonal to the $\mathbf{k}$ vector, the direction of emission is 100% modulated by the photon polarization (i.e., the angular distribution (1), integrated over the variable θ, is proportional to $\cos^2\phi$).

In Fig. 2 a schematic view of a micro pattern gas detector (MPGD) [7], [8] designed for polarimetric applications is shown. A photon enters the detector through a thin drift window and it is absorbed somewhere in the upper gas filled gap. The photoelectron is emitted preferentially around its direction of polarization and leaves along its path a string of ion-electron pairs; the ions and electrons are separated and transported by the drift field. The gas electron multiplier (GEM) [9] provides amplification for the primary ionization and a trigger for readout electronics. It consists of a thin (50 μm) insulating foil,

Manuscript received December 7, 2001; revised February 13, 2002. This work was supported in part by Agenzia Spaziale Italiana (ASI).

R. Bellazzini, A. Brez, L. Latronico, N. Lumb, and G. Spandre are with the Istituto Nazionale di Fisica Nucleare, Sezione di Pisa, I-56010 San Piero a Grado, Italy (e-mail: ronaldo.bellazzini@pi.infn.it).

F. Angelini, L. Baldini, and M. M. Massai are with the Istituto Nazionale di Fisica Nucleare, Sezione di Pisa, 56010 Pisa, Italy, and also with Universitá degli Studi di Pisa, 56010 Pisa, Italy.

N. Omodei is with the Istituto Nazionale di Fisica Nucleare, Sezione di Pisa, 56010 Pisa, Italy, and also with Universitá degli Studi di Siena, 53100 Siena, Italy.

E. Costa and P. Soffitta are with the Istituto di Astrofisica Spaziale del CNR, I-00133 Rome, Italy.

Publisher Item Identifier S 0018-9499(02)06104-X.

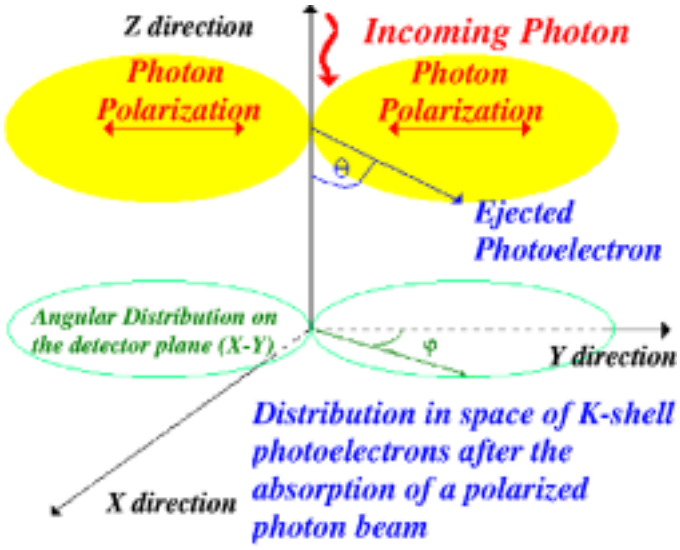

Fig. 1. Photoelectric effect: when incoming photons are linearly polarized, photoelectrons are ejected preferentially around the polarization direction of the photons (y axis in figure).

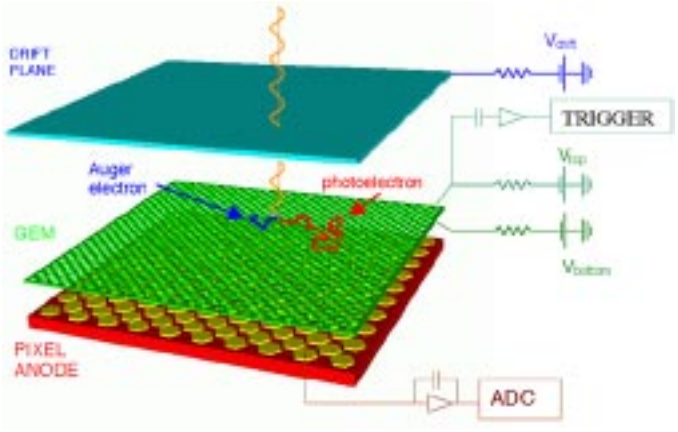

Fig. 2. The MPGD. Readout plane is grounded, while both sides of GEM and drift plane are at increasingly negative high voltages. Far from the GEM the electric field is approximately uniform and directed toward the drift plane. The charge released by the photoelectron is amplified and then collected by readout pixels, each one connected to an independent electronic chain.

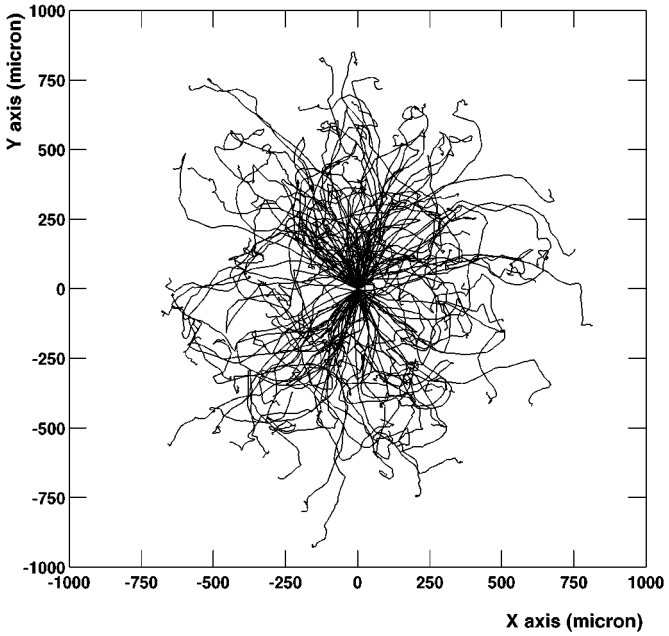

Fig. 3. Simulated tracks produced by 4.6-keV photoelectrons emitted from a 100% polarized source in pure Ne. Information about the direction of emission resides in the initial part of each track.

metallized on each side, etched with a regular matrix of holes; the application of a suitable potential difference between the electrodes gives rise to an intense dipole field inside the holes sufficient to induce avalanche multiplication. The focusing effect of the field provides high efficiency for charge transfer, while the small pitch of the matrix of holes (50–100 μm) allows high granularity to be achieved in both dimensions. The polarization information is derived from the tracks of the photoelectrons reconstructed on the pixel readout plane; the total charge collected on the anode is proportional to the energy released, so that the MPGD provides also information about photon energy. An alternative approach tried by other groups [10], [11] could consist in the collection of the light (instead of the charge) produced in the avalanche.

The photoelectron interacts with the gas mixture basically through ionization and Coulomb scattering. The energy loss due to ionization is well described by a modified Bethe law, valid in the keV regime

$$\frac{dE}{dx} \propto \varrho \frac{Z}{A} \frac{1}{E} \ln \left[\frac{1.166(E+0.85J)}{J} \right] \tag{2}$$

where ϱ, Z, A, and J are, respectively, density, atomic number, mass number, and mean excitation potential of the gas and E is the kinetic energy of the electron. The energy loss is proportional to $1/E$, i.e., the particle releases most of its energy toward the end of its path. The elastic scattering on atomic nuclei follows the screened Rutherford formula

$$\frac{d\sigma}{d\Omega} \propto \frac{Z^2}{E^2} \frac{1}{(\sin^2 \theta/2 + \alpha_{\text{screen}})}. \tag{3}$$

The mean scattering angle is large at low energy so that electron scattering is responsible for a progressive randomization of the photoelectron direction (Fig. 3); that is, most of the information about the original direction of emission resides in the initial part of the electron track. We notice also that while slowing down (energy loss due to ionization) is proportional to Z, the Rutherford cross section goes as Z^2; the straightness of the photoelectron path depends on the stopping power/scattering ratio, which decreases with Z. In this sense, low Z gas mixtures are, in principle, better; furthermore, they have low-energy K-edges so that the Auger electron, which is emitted isotropically, carries only a small fraction of the original photon energy and does not blur the directional information. For our application, the price to pay is obviously a lower detection efficiency.

III. Results

In Fig. 4 the fully assembled tested detector is shown; the charge collection plane consists of 200 μm-pitch hexagonal pixels [Fig. 5(b)] and the connection to the readout electronics is made with a multilayer printed circuit board (PCB) fan out;

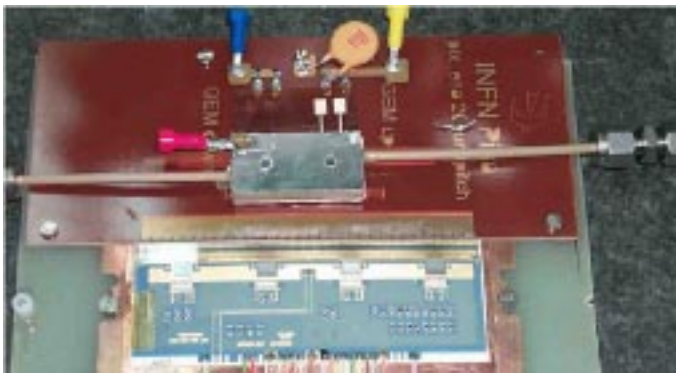

Fig. 4. The overall detector assembly and readout electronics. The absorption gap is 6 mm thick, while the distance between GEM and the collection plane is 1.5 mm.

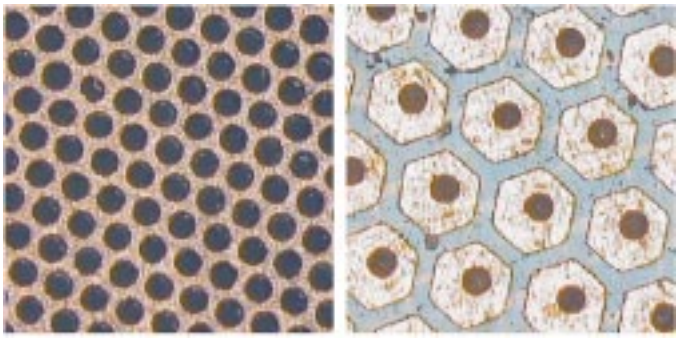

(a) (b)

Fig. 5. Microscope pictures of the current MPGD prototype. (a) The GEM (50-μm-thick matrix, 90-μm pitch holes). (b) The readout plane (200-μm pitch hexagonal pixels).

we underline the fact that we separately read 512 electronic channels from a few mm^2 active area. Fig. 5(a) shows a microscope picture of the gas electron multiplier (GEM).

We have tested the detector with both unpolarized radiation (5.9-keV ^{55}Fe source) and polarized X-rays; polarized photons are obtained by Thomson scattering at 90° of the photons produced by an X-ray tube with a Cu (8.04 keV) or Cr (5.4 keV) anode. A 1-atm Ne-DME 80/20 mixture (80% Ne, 20% dimethyl ether) was used throughout the measurements described in this work. Even in such a light gas mixture, a 5-keV photoelectron track is only a few hundred micrometers long.

Fig. 6 shows a sample of real photoelectron tracks (from a run with ^{55}Fe source) as imaged by the current MPGD prototype. In traditional position-sensitive gas detectors the extent of the charge cloud is typically the ultimate limit to the spatial resolution and it is usually kept as small as possible; our approach here is exactly the opposite: thanks to the large number of fired pixels per event we are able to *resolve* the track of the photoelectron and extract the directional information it carries. It is easy to see that the ionization density is not uniform: most of the charge is released toward the end of the track, according to (2); it is also evident that large-angle Rutherford scatterings can occur [Fig. 6(d)]. We notice that the charge distribution is smoothed by the transverse diffusion of the primary ionization during the drift from the conversion point to the readout plane. Then, the absorption gap cannot be too thick; 1 cm at standard pressure is a good compromise between diffusion and detection

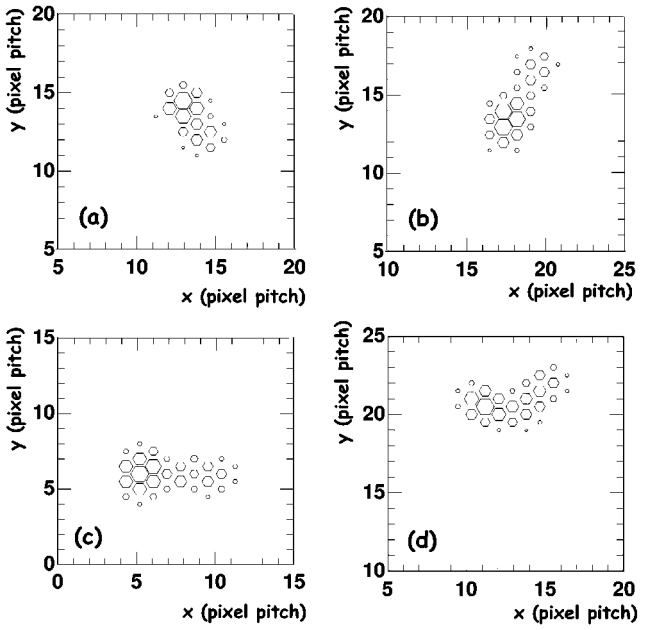

Fig. 6. Real tracks of photoelectrons from 5.9-keV unpolarized photons in a 1-atm Ne/DME 80/20 gas mixture, obtained with the current MPGD prototype; the area of each hexagon is proportional to the charge released in the corresponding pixel. The final part of the track is characterized by a larger ionization density. (a), (b), (c) Typical photoelectron tracks. (d) Track in which a large scale coulomb scattering has occurred.

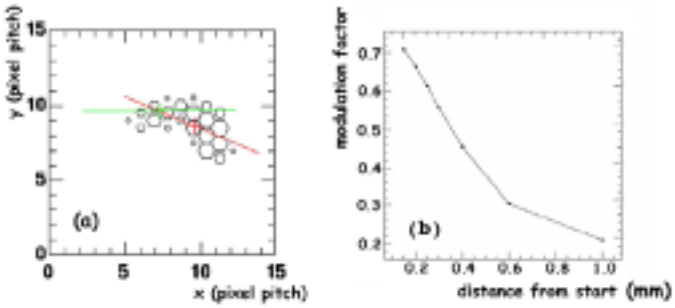

Fig. 7. (a) Real photoelectron track in a 1-atm Ne/DME 80/20 mixture, obtained with the current MPGD prototype from a run with 5.4-keV polarized radiation. In this case, the path of the electron has been seriously affected by Coulomb scattering on a nucleus so that the mean direction of the track (red line) is quite different from the starting direction. A better reconstruction of the direction is obtained at the second pass of the reconstruction algorithm (green line) after conversion point identification and removal of the final part of the track. (b) Here it is shown how the modulation factor (5) depends on the track length used in the reconstruction (for 5-keV simulated photoelectrons in pure Ne at 1 atm).

efficiency, while a further increase of the latter can be achieved only by a parallel increase of the gas pressure.

The reconstruction of the polarization angle is a two-stage process. At the simplest level, we reconstruct the angle of emission of the photoelectron by finding the principal axes of the charge distribution, i.e., the two (orthogonal) directions for which the second moment of the charge pattern (with respect to its barycenter) are maximum and minimum. The major principal axis [red line in Fig. 7(a)] can be identified to first order with the photoemission direction. At the second stage, we calculate the third momentum of the charge distribution along the major principal axis itself; this gives an idea of the

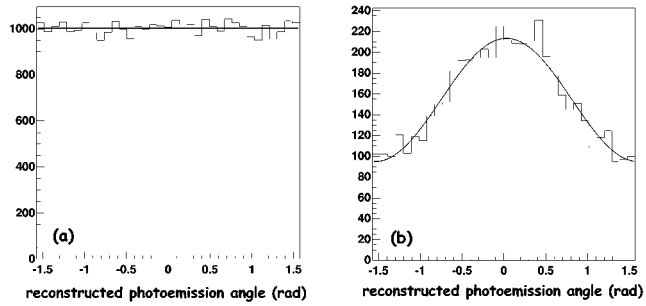

Fig. 8. Cluster angular distribution for (a) 5.9-keV unpolarized and (b) 5.4-keV polarized radiation in a 1-atm Ne/DME 80/20 mixture, obtained with the current MPGD prototype. While in the first case, the distribution is flat, in the second, it is peaked around the polarization angle of the incident beam (0° in this run). The modulation factor with the applied cuts is ≃40%.

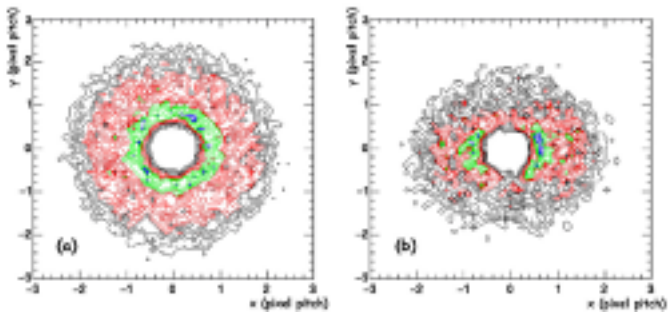

Fig. 9. Distribution of track barycenters with respect to (a) the photoelectron starting point for 5.9-keV unpolarized and (b) 5.4-keV polarized radiation. The asymmetry in the second case is clearly visible.

asymmetry of charge release. Since the ionization density is lower toward the start of the track, this approach allows us to find an estimate for the absorption point that is much more accurate than the barycenter of the cluster. This provides both an improvement in the imaging capabilities of the detector and an enhancement in angular reconstruction accuracy since it allows us to reject the pixels fired near the end of the track, where the path is more randomized [the result is the green line in Fig. 7(a)]. Fig. 8 shows the angular distributions of the tracks for 5.9 keV unpolarized radiation (^{55}Fe source) and for 5.4-keV 100% polarized photons (X-ray tube with Cr anode); in the first case, the distribution is flat, while in the latter, it is well modeled by

$$N(\phi) = C_1 + C_2 \cos^2(\phi - \phi_{\rm pol}) \tag{4}$$

in which the modulated term derives from (1), while the constant term is due to the randomization induced by electron scattering. We also notice that in the case of polarized radiation, the distribution of track barycenters with respect to the reconstructed conversion point is clearly asymmetrical [see Fig. 9(b)]. The visibility of the modulation for 100% linearly polarized incident radiation

$$\mu = \frac{N_{\rm max} - N_{\rm min}}{N_{\rm max} + N_{\rm min}} = \frac{C_2}{2C_1 + C_2} \tag{5}$$

is a fundamental parameter of the instrument called the modulation factor; for $\mu = 0$ the instrument is insensitive to polarization, while $\mu = 1$ implies a perfect analyzer.

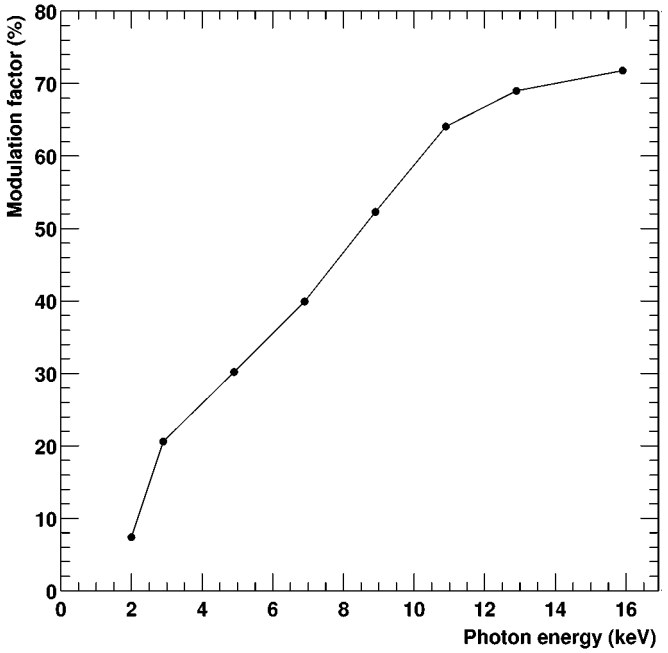

Fig. 10. Modulation factor (with no cuts on events) as a function of X-ray energy simulated for our prototype configuration (Figs. 4 and 5) and gas mixture (Ne/DME 80/20), but with a 100-μm pitch readout plane and 1-cm-thick absorption gap.

The performance of a polarimeter is usually expressed in terms of minimum detectable polarization (MDP), which is simply the minimum modulated flux needed to exceed at the desired level of confidence, the expected statistical fluctuations both of the background, and of the unpolarized fraction of the source; at the level of n_σ standard deviations, it is given by [8]

$$\mathrm{MDP}(n_\sigma) = \frac{n_\sigma}{\epsilon \mu F} \sqrt{\frac{2(B + \epsilon F)}{ST}} \tag{6}$$

where F is the source flux, ϵ the detector efficiency, B the background rate per unit of surface, S the collecting area (eventually the effective area of the optics), and T the observing time. More exactly, since μ, F, B, and ϵ (and A, if the instrument is placed at the focus of grazing incidence optics) are energy dependent quantities, (6) must be integrated over the energy range of interest; so knowing how μ depends on X-ray energy is of crucial importance.

In order to do that, we have developed a Monte Carlo simulation [8] that starting from the distribution (1) takes into account the interaction of the photoelectron with the gas, the diffusion of the primary ionization, the multiplication in GEM holes and the collection on the readout plane; the results of the simulation are in good agreement with experimental data.

Fig. 10 shows the results of the simulation for a 100 μm pitch readout plane, which is now under construction and will soon be ready to be tested; as we expect, there is a significant improvement with respect to the current prototype especially at low energies, where the electron range is smaller; this point is particularly important because at low energies, source spectra are more populated and X-ray optics are more efficient.

A 100-μm-pitch readout is probably near to the limit of our PCB technology. The real step forward will be the realization

TABLE I
GAIN OVER THE TWO SXRP STAGES (IN TERMS OF INTEGRATION TIME) FOR OUR CURRENT MPGD PROTOTYPE (200-μm-PITCH READOUT PLANE, 6-mm ABSORPTION GAP, AND 1-atm Ne/DME 80/20) AND FOR ONE OF THE POSSIBLE OPTIMIZED CONFIGURATIONS (50-μm-PITCH READOUT PLANE, 30-mm ABSORPTION GAP, AND 4-atm Ne/DME 40/60)

Gain over SXRP			
Sources	SXRP Polarimeter	Current MPGD	Optimized MPGD
Strong	Bragg	15	300
Strong	Thomson	5	100
Faint	Bragg	100	2000
Faint	Thomson	250	5000

of a very large scale integration (VLSI) readout plane with integrated front-end electronics; this will mean smaller pitch (50 μm or less), no problems with the fan out, and essentially no limit in the number of channels.

The Stellar X-ray polarimeter (SXRP) is, to date, the only planned experiment dedicated to nonsolar X-ray sources with polarimetric capabilities. It exploits the two conventional techniques of X-ray polarimetry (Bragg diffraction at 45° and Thomson scattering at 90° [8]) and it should fly aboard SXG (Spectrum X Gamma) mission [12] at the focus of the Sodart X-ray optics. We have evaluated the performance that the present detector and an improved configuration (50-μm-pitch readout plane, 30-mm absorption gap filled with a Ne/DME 40/60 gas mixture at 4 atm) would have at the focus of Sodart. The gain, in terms of integration time, with respect to the two polarimeters (Bragg and Thomson) of SXRP is shown in Table I for strong $(F \gg B)$ and faint $(F \ll B)$ sources [see (6)].

IV. CONCLUSION

Our results clearly show the feasibility of a new generation of high-efficiency X-ray polarimeters for the 2–10 keV energy band. The MPGD is nondispersive and, being truly two dimensional, it does not require rotation (while standard polarimeters do); at the same time it produces good images (50–100 μm spatial resolution at 5.4 keV) and moderately good spectroscopy (20% full width at half maximum (FWHM) at 5.4 keV). The performances of the tested prototype (not optimized for astrophysical use) are much better than those of SXRP, which represents the state of the art in traditional X-ray polarimetry. In its improved configuration, the MPGD target performance is the detection of 1% polarization for 1-m Crab sources (i.e., sources whose flux is 1000 times smaller than that of the Crab). This sensitivity will allow polarimetry measurements to be made on thousands of galactic and extragalactic sources: a real breakthrough in X-ray astronomy.

REFERENCES

[1] R. A. Sunyaev and L. G. Titarchuk, "Comptonization of low frequency radiation in accretion disks: Angular distribution and polarization of hard radiation," *Astron. Astrophys.*, vol. 143, pp. 374–388, 1985.
[2] R. F. Stark and P. A. Connors, "Observable gravitational effects on polarized radiation coming from near a black hole," *Nature*, vol. 269, pp. 128–129, 1977.
[3] T. Kii, "X-ray polarizations from accreting strongly magnetized neutron stars: Case studies for the X-ray pulsars 4U 1626-67 and hercules X-1," *Publ. Astron. Soc. Japan*, vol. 39, pp. 781–800, 1987.
[4] P. Meszaros, R. Novick, G. A. Chanan, M. C. Weisskopf, and A. Szentgyorgyi, "Astrophysical implications and observational prospects of X-ray polarimetry," *Astrophysical J.*, vol. 324, pp. 1056–1067, 1988.
[5] M. C. Weisskopf, G. G. Cohen, H. L. Kenstenbaum, K. S. Long, R. Novick, and R. S. Wolff, "Measurement of the X-ray polarization of the Crab Nebula," *Astrophysical J.*, vol. 208, pp. L125–L128, 1976.
[6] W. Heitler, *The Quantum Theory of Radiation*. Oxford, U.K.: Oxford Univ. Press, 1970.
[7] E. Costa, P. Soffitta, R. Bellazzini, A. Brez, N. Lumb, and G. Spandre, "An efficient photoelectric X-ray polarimeter for the study of black holes and neutron stars," *Nature*, vol. 411, pp. 662–664, 2001.
[8] P. Soffitta, E. Costa, G. di Persio, E. Morelli, A. Rubini, R. Bellazzini, A. Brez, R. Raffo, G. Spandre, and D. Joy, "Astronomical X-ray polarimetry based on photoelectric effect with microgap detectors," *Nucl. Instrum. Methods*, vol. A. 469, pp. 164–184, 2001.
[9] F. Sauli, "GEM: A new concept for electron amplification in gas detectors," *Nucl. Instrum. Methods*, vol. A. 386, pp. 531–534, 1997.
[10] H. Sakurai, T. Tamura, S. Gunji, and M. Noma, "A new type of proportional counter using a capillary plate," *Nucl. Instrum. Methods*, vol. A. 374, pp. 341–344, 1996.
[11] A. La Monaca, E. Costa, P. Soffitta, G. Di Persio, M. Manzan, B. Martino, G. Patria, G. Cappuccio, and N. Zema, "A new photoelectron imager for X-ray astronomical polarimetry," *Nucl. Instrum. Methods*, vol. A. 416, pp. 267–277, 1998.
[12] P. Kaaret, J. Schwartz, P. Soffitta, J. Dwyer, P. Shaw, and S. Hanany *et al.*, "Status of the stellar X-ray polarimeter for the spectrum X-gamma mission," *Proc. SPIE*, vol. 2010, pp. 22–27, 1993.